# Degradation Mode Knowledge Transfer Method for LFP Batteries

Xin Lu, *Student Member*, *IEEE*, Jing Qiu, *Senior Member*, *IEEE*, Gang Lei, *Member*, *IEEE*, Jianguo Zhu, *Senior Member*, *IEEE*

***Abstract*-- Lithium-ion (Li-ion) batteries are widely utilized as energy storage units owing to their high energy density and safety. However, when battery degradation occurs, Li-ion batteries deteriorate and become untrustworthy. Accurate diagnosis and identification of the degradation modes constitute a critical task for systems employing Li-ion batteries. Current diagnosis methods are usually post-analysis and cannot be directly employed for diagnosing the batteries that are in operation. This study proposes a ResNet-50 based diagnosis model for degradation modes, which can quantify the contribution of three degradation modes for the synthetic datasets. Because the real and synthetic datasets are independent and identically distributed, it is difficult to apply this model to the real datasets. To bridge the gap, this paper proposes a deep domain adaptation method to minimize the classification loss and domain adaptation loss between the source domain (synthetic) and the target domain (real) such that the degradation knowledge learned from the synthetic batteries can be transferred to the real batteries. The model's input, structure, and parameters are optimized through simulation tests to improve the diagnosis accuracy. A validation session is designed to verify the classification accuracy of unlabeled degradation modes of the lithium iron phosphate (LFP) battery. The results show that the proposed method can effectively transfer the knowledge of degradations from synthetic batteries to real-world LFP batteries to diagnose and identify degradation modes of LFP batteries with relatively high classification accuracy.**

***Index Terms*-- Li-ion Battery; Degradation; Diagnosis Model; Domain Adaptation; Transfer Learning.**

NOMENCLATURE:

Parameters

| | |
|---|---|
| $dQ/dV$ | Differential capacity |
| $\Delta Q(V)$ | Cycle-to-cycle evolution of capacity |
| $\mathcal{D}^{\mathcal{S}}$ | Source domain |
| $\mathcal{D}^{\mathcal{T}}$ | Target domain |
| $\mathcal{F}(\cdot)$ | Classification model for DMs |
| $\boldsymbol{X}^{\mathcal{S}}$, $\boldsymbol{Y}^{\mathcal{S}}$ | Feature and the label space of the source domain |
| $\boldsymbol{X}^{\mathcal{T}}$, $\boldsymbol{Y}^{\mathcal{T}}$ | Feature and the label space of the target domain |
| $C^{\mathcal{S}}$, $C^{\mathcal{T}}$ | Feature covariance matrices of source/target domains |
| $\ell_{coral}$ | DeepCoral loss |
| $\ell_{class}$ | Classification loss |
| $\boldsymbol{X}_{ij}^{\mathcal{S}}$, $\boldsymbol{X}_{ij}^{\mathcal{T}}$ | $j$-th dimension of the $i$-th source and target data |
| $N^{correct}$ | Number of correct classifications |
| $N^{total}$ | Total number of samples in the test set |

Abbreviations

| | |
|---|---|
| BESS | Battery energy storage system |
| BNM | Batch nuclear-norm maximization |
| C-rate | Current rate |
| CNN | Convolutional neural network |
| DANN | Dynamic adversarial adaptation network |
| DAN | Deep adaptation network |
| DSAN | Deep subdomain adaptation network |
| DL | Deep learning |
| DM | Degradation mode |
| DMDM | DM diagnosis model |
| DV | Differential voltage |
| EM | Electrochemical model |
| EV | Electric vehicle |
| IC | Incremental capacity |
| $LAM^{PE}$ | Loss of active positive electrode materials |
| $LAM^{NE}$ | Loss of negative electrode materials |
| LFP | Lithium iron phosphate |
| LLI | Loss of lithium inventory |
| Li-ion | Lithium-ion |
| LMMD | Local MMD |
| LSTM | Long short term memory |
| ML | Machine learning |
| MMD | Maximum mean discrepancy |
| NCA | Nickel cobalt aluminum |
| NMC | Nickel manganese cobalt |
| ResNet | Residual neural network |
| RNN | Recurrent neural network |
| SEI | Solid electrolyte interphase |
| SOH | State of health |
| VPP | Virtual power plant |

X. Lu, J. Qiu and J. Zhu are with the School of Electrical and Information Engineering, The University of Sydney, Darlington 2008, New South Wales, Australia (e-mail: xin.lu@sydney.edu.au; jeremy.qiu@sydney.edu.au; jianguo.zhu@sydney.edu.au)

G. Lei is with School of Electrical and Data Engineering, University of Technology Sydney, Ultimo 2007, New South Wales, Australia (e-mail: gang.lei@uts.edu.au)

## I. Introduction

Li-ion batteries are a prevalent group of energy storage devices because of their high energy density and safety, long lifetime, and low self-discharge rate [1, 2]. They have been widely utilized in many electrical applications, such as electric vehicles (EVs) [3], battery energy storage systems (BESS) [4], and virtual power plants (VPPs) [5, 6]. However, an unexpected failure or exposure to environmental conditions can degrade the performance of batteries [7, 8], which affects the batteries' energy storage ability and leads to their end of life. For systems that employ Li-ion batteries, the amount of energy that can be stored and the power that can be provided should be monitored at any point in time. Therefore, many studies have been conducted on the estimation of the states of health (SOH) of Li-ion batteries with the remaining capacity as the indicator. However, the remaining capacity is a result that can be attributed to various types of degradations, and the same amount of remaining capacity may result from different degradations. Finding out the degradation of Li-ion batteries is difficult currently and can help identify and understand the SOH of the battery more accurately.

Degradation in Li-ion batteries is caused by various physical and chemical factors that affect the electrodes, the electrolyte, the separator, and the current collectors. Generally, the degradation modes (DMs) in Li-ion batteries can be divided into three broad modes: loss of lithium inventory (LLI), loss of active positive electrode materials ($LAM^{PE}$), and negative

electrode materials ($LAM^{NE}$) [7, 9]. LLI occurs because lithium ions are consumed by the parasitic reaction, such as film formation, decomposition reactions, and lithium plating, and are no longer available for cycling. Due to particle cracking or loss of electrical contact or blocking of active sites by resistive surface layers, the active mass of the anode is no longer available for the lithium insertion, which leads to the $LAM^{PE}$. The same phenomena also appears in the cathode due to structural disordering, particle cracking, or loss of electrical contact, which is called $LAM^{NE}$. While LLI only causes capacity fade, $LAM^{PE}$ and $LAM^{NE}$ cause both capacity fade and power fade. Because of the complex failure mechanisms, it is challenging to identify and quantify the degradation of batteries in operation [10].

Physics-based models can capture DMs on a micro-scale, such as a particle or molecular level, and focus only on the main dominant mechanisms, such as the formation of the solid electrolyte interphase (SEI) or electronic contact loss through particle cracking [11], due to various complex causes and interdependencies of these degradation mechanisms [7]. However, physics-based models are always used with post-mortem analysis methods. These methods can identify the causes of battery degradation and failure but cannot provide effective temporal resolution for the actual battery monitoring and diagnosis during operation [12]. A chemical/mechanical degradation model was proposed by J. Li et al. [13]. This model can predict the capacity fade with multiple degradation mechanisms during cycling quickly. However, the study was conducted by analyzing the SEI layer formation [11] with some ideal parameters like particle size and temperature. It is hard to apply this method in real-world batteries. R. Xiong et al. [14] proposed an electrochemical model (EM) to identify the degradation state and analyze the degradation trajectories at different temperatures. Similar to the chemical/mechanical models aforementioned, this model is only applicable to a specific ideal environment but cannot be applied to the complex and changing real world. Incremental capacity (IC) analysis and differential voltage (DV) analysis techniques can obtain the change of degradation by applying the peaks of curves. However, the IC and DV curves are generally obtained with a relatively low charging current rate (C-rate), and the IC curves in the real world with high C-rate tend to lose much useful information [2]. Besides these conventional methods, machine learning (ML) methods are attracting more and more attention in investigating degradation mechanisms. Y. Zhang et al. [15] employed ML with electrochemical impedance spectroscopy (EIS) to predict the remaining useful life. Using ML, multiple impedance-related features were extracted from the charging curves and correlated with the degradation phenomenon [16]. Still, these data-driven methods cannot identify DMs directly. S. Kim et al. [17] built a DM classification framework with deep learning (DL). K. Mayilvahanan et al. [18] proposed a supervised degradation diagnosis framework with features extracted from IC curves under low C-rate with random forest regressors. However, these two frameworks were validated by synthetic datasets. Whether it can work effectively with real-world battery datasets under variable environmental influences has not been verified. In addition, due to the difficulty of obtaining DM, there is currently no real-world dataset with DM labels for direct diagnosis with ML and DL. Matthieu et al. proposed a mechanistic approach combines both modeling and experimental techniques to generate big synthetic data for the degradations of Li-ion batteries [19, 20]. However, due to the distribution differences between synthetic and real dataset, there is a lack of an effective method to apply these big data to diagnose real batteries under different conditions.

Since conventional ML methods require that the training and testing samples are independent and identically distributed, it is difficult to apply the approach in [12] to real datasets. In the real world, batteries are generally operated in complex and variable environments, such as electric vehicles with significant temperature differences between day and night and complex energy recycling systems with frequent automatic charging and discharging. It is impossible to obtain the battery data under the same operating environmental conditions. Transfer learning has been introduced in battery state of charge estimation [21] and capacity estimation [22, 23] and can provide us with a perspective to solve this problem that the test set and training set are distributed differently. By transferring the learned knowledge from one battery dataset to another with different operations and environments, and the learned degradation can be transferred from one area (the source domain) with labeled data to another area (the target domain) with unlabeled data. However, directly fine-tuning the parameters of DL networks is problematic because of the representation bias in the distribution of the source and target domains [24]. It is crucial to optimize the domain invariance to improve the feature transferability by finding a representation that can make the domains similar while simultaneously reducing the domain discrepancy.

In this work, a quantitative DM diagnosis problem for the LFP battery is first proposed. We propose a novel DM classification architecture with knowledge transferability to label the DMs for unlabeled real dataset. The main contributions of this work are as follows:

1) A quantitative DM diagnosis problem for LFP batteries is first proposed to describe the degradation of Li-ion batteries classification problem.
2) A novel $\Delta Q(V)$ image-based DM diagnosis model (DMDM) is proposed to classify the DMs, which can effectively extract image-based features and improve the classification accuracy.
3) A deep domain adaptation method is proposed to solve the DM diagnosis problem by optimizing the classification loss on a labeled dataset and domain adaptation loss on the source and target domains.
4) The proposed method can transfer the DM knowledge not only within the synthetic dataset but also from the synthetic dataset to the real dataset across different LFP types.

## II. Problem Statement

### A. Degradation Modes of LFP Battery

The degradation of Li-ion batteries is a complex process

caused by multiple mechanisms. For simplicity, the aging mechanisms can be categorized into three DMs: LLI, $LAM^{PE}$, and $LAM^{NE}$ [9]. These DMs can usually be observed by analyzing the charging or discharging curves with a small C-rate. The DMs obtained by this analysis method are usually qualitative rather than quantitative. In practice, charging or discharging at a low C-rate of C/25 is unreasonable and can cause battery regeneration, affecting the SOH estimation results. Matthieu and David [19] from the University of Hawaii generated the first comprehensive synthetic dataset (>700,000 unique curves) with 'alawa' toolbox in MATLAB environment [25], considering the capacity loss under various degradation models. With this publicly available dataset, a data-driven DMDM can be readily obtained through ML. However, the key issue is how to apply the DM knowledge that DMDM learned from the synthetic dataset to diagnose the real LFP batteries.

### *B. Domain Adaptation for Degradation Modes*

Taking into account all factors (LAMs, LLI, polarization, phases, temperature, and so on .....) of all possible evolutions (linear, exponential, delay, etc.) requires enormous computing time and will generate overwhelming datasets. The DMs from the synthetic and real battery datasets are different in distributions. This discrepancy of distributions between the representations of the source (synthetic) dataset and target (real) dataset becomes a major obstacle to applying DMDM across domains directly. By exploring the domain-invariant features that bridge different domains of substantial distribution discrepancy, the domain adaptation process can help transfer the knowledge learned from the labeled source domain to the unlabeled target domain. In this work, we make a first attempt to transfer the knowledge of DMs from synthetic datasets to real datasets, which will help to quickly and efficiently label DMs under different conditions, such as temperature, C-rate in real datasets.

The capacity loss is only an indicator of the battery SOH, and even the same capacity loss may be due to a combination of different DMs. Identification and diagnosis of LLI, $LAM^{PE,}$ and $LAM^{NE}$ can enable a correct assessment of the SOH. Dubarry et al. [12] mapped DMs to their resultant shift in $dQ/dV$ and $dV/dQ$ derivatives for diagnostic cycles at C/20. However, as proposed in [26], the shift in $dQ/dV$ cannot be conveniently observed at high charging C-rate, and cycle-to-cycle evolution of $\Delta Q(V)$ is proposed to capture the electrochemical evolution of individual battery during cycling, and this transformation is of particular interest because the voltage curves and their derivatives are a rich data source that is effective in degradation diagnosis [27, 28]. Let $\Delta Q_{C-1}(V) = Q_C(V) - Q_1(V)$ denotes the change in charging voltage curves between cycle C and the initial cycle and $DM_C = \{LLI_C, LAM_C^{PE}, LAM_C^{NE}\}$ denotes the DMs in cycle C. The DMDM can be expressed as a supervised classification model $\mathcal{F}(\Delta Q_{C-1}(V), DM_C)$, and can be trained by the labelled synthetic DMs dataset. However, the performance of this model is generally unsatisfactory on the DMs which are not presented in the training dataset or the DMs of real battery dataset. This is because the distribution discrepancy between the training dataset and the testing dataset. To this end, we use the domain adaptation method to make full use of the unlabeled dataset, and thus the model transferability from training dataset to unpresented dataset or real dataset can be improved.

Suppose that the source domain dataset from a cycle $\mathcal{D}^{\mathcal{S}} = \{(\Delta Q_{2-1}(V)^{\mathcal{S}}, {DM_2}^{\mathcal{S}}), \cdots (\Delta Q_{i-1}(V)^{\mathcal{S}}, {DM_i}^{\mathcal{S}}), \cdots (\Delta Q_{n_{\mathcal{S}}-1}(V)^{\mathcal{S}}, {DM_{n_{\mathcal{S}}}}^{\mathcal{S}})\}$ includes the labeled DMs, and the target domain dataset $\mathcal{D}^{\mathcal{T}} = \{\Delta Q_{2-1}(V)^{\mathcal{T}}, \cdots \Delta Q_{i-1}(V)^{\mathcal{T}}, \cdots \Delta Q_{n_{\mathcal{T}}-1}(V)^{\mathcal{T}}\}$ includes the unlabeled DMs, where $\Delta Q_{i-1}(V)^{\mathcal{S}} \epsilon \boldsymbol{X}^{\mathcal{S}}$ is the input charging curve of domain source, ${DM_i}^{\mathcal{S}} \epsilon \boldsymbol{Y}^{\mathcal{S}}$ the labeled output DMs of domain source, and $\Delta Q_{i-1}(V)^{\mathcal{T}} \epsilon \boldsymbol{X}^{\mathcal{T}}$ the unlabeled input charging curve of target source. The number of source and target datasets are $n_{\mathcal{S}} - 1$ and $n_{\mathcal{T}} - 1$, respectively. The feature space and the label space of the source domain are denoted as $\boldsymbol{X}^{\mathcal{S}}$ and $\boldsymbol{Y}^{\mathcal{S}}$, respectively, and the feature space of the target domain is denoted as $\boldsymbol{X}^{\mathcal{T}}$. The domain distribution is commonly defined as the marginal probability of feature space [29]. However, the marginal probability of feature space in the source domain is different from that in the target domain, i.e., $P^{\mathcal{S}}(\boldsymbol{X}^{\mathcal{S}}) \neq P^{\mathcal{T}}(\boldsymbol{X}^{\mathcal{T}})$ [30]. Directly applying the model $\mathcal{F}(\boldsymbol{X}^{\mathcal{S}}, \boldsymbol{Y}^{\mathcal{S}})$ to target domain may generate significant error, since it does not consider the distribution characteristics of target domain. To address this problem, it is necessary to train a DMDM classification model $\mathcal{F}(\boldsymbol{X}^{\mathcal{S}}, \boldsymbol{Y}^{\mathcal{S}}, \boldsymbol{X}^{\mathcal{T}})$, which contains both labelled source domain and unlabeled target domain, and the DM knowledge transferability can be enhanced by reducing the discrepancy between source and target domains.

## III. Model Framework

This section presents the proposed methodology of DMDM. The conventional qualitative analysis methods tend to calculate the curves of Q and V to obtain the images of IC curves and determine DMs by analyzing whether the peaks or valleys of these IC curve images are shifted left or up. In recent years, some ML methods exploring the health of batteries typically use these curves but often as input in the form of a one-dimensional sequence [17]. However, this approach results in the loss of some image features when the two-dimensional image is converted into a one-dimensional sequence, which eventually leads to inaccurate results. In this paper, we choose to use $\Delta Q(V)$ images as the input so that the ML can better identify useful features. The network architecture for DMDM is given in Fig. 1.

A deep network of residual neural network (ResNet) is introduced to learn a deep representation that is both source and target domain invariants and can offer strong separation ability. Then, the supervised DMDM loss can be calculated by using the labeled source, while the domain adaptation loss is obtained by comparing the distance between the source and target domain distributions. A deepCoral loss is combined to determine the neural network weights by backpropagation training. Note that the weights of parameters are shared between the source and target domains. The network is jointly trained to minimize the total loss. Each part of the proposed framework is described in the following subsections.

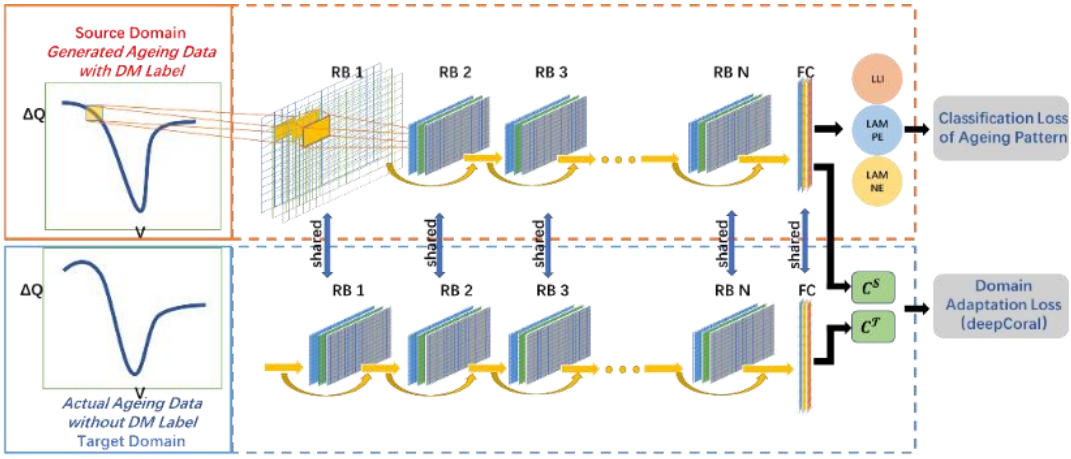


Fig. 1. The architecture of the proposed deep domain adaptation for DMDM

### A. ResNet-50

The ResNet is a type of deep convolutional neural network architecture composed of a series of residual blocks [31]. A residual block is made up of several conventional layers and an identity mapping "skip" connection $a^{[l]}$ that can pass over layers to a deeper location in the ResNet. The skip connection in the ResNet architecture makes it uniquely applicable to the DM problem. The original features of $\Delta Q(V)$ images can be captured by the traditional connections between layers in the ResNet, and the "skip" connection enables the ResNet to learn the complex impacts behind the peaks and valleys but skip the unnecessaries that are not the main useful features. This is the reason why the "skip" connection can enable ResNet to capture the complex second-order relationship from the original $\Delta Q(V)$ images and classify the DMs without forcing the model to overfit a single layer and cause problems of vanishing gradients or accuracy saturation degradations [32].

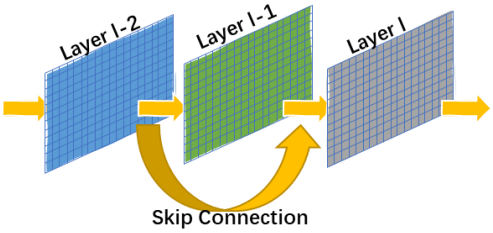


Fig. 2. The residual blocks with skip connection

The conventional forward propagation through the activation function can be expressed as follows:

$$Z^{[l]} = W^{[l-1,l]} * a^{[l-1]} + B^{[l]} \quad (1)$$

$$a^{[l]} = f\left(Z^{[l]}\right) \quad (2)$$

where $W^{[l-1,l]}$ is the weight matrix for neurons between layer $l-1$ and $l$, $B^{[l]}$ the biases, $a^{[l-1]}$ the activations outputs of neurons in layer $l$, and $f(\cdot)$ denotes the activation function for layer $l$. As shown in Fig. 2, when the skip connection is introduced, the original input information $a^{[l-2]}$ is added before the next non-linearity function as follows:

$$a^{[l]} = f\left(Z^{[l]} + a^{[l-2]}\right) \quad (3)$$

$$a^{[l]} = f(W^{[l-1.l]} * a^{[l-1]} + B^{[l]} + a^{[l-2]}) \quad (4)$$

Except for the convolution layers and the skip connection, the batch normalization layers are often included as part of the ResNet to accelerate the learning speed and ensure the stability of the training process. The specific architecture of a ResNet can vary depending on the application with different numbers and types of layers. In this work, ResNet-50 is chosen for the proposed DM classification problem with fast computing speed, sufficiently adjustable parameters, and outstanding classification performance.

### B. DeepCoral Loss

For effective deep domain adaptation transfer learning, the distribution discrepancy between the source and target domains should be reduced to learn the domain invariance representation. Many unsupervised adaption approaches are explored to measure the data distribution distances. The deepCoral loss was proposed in [33] and can be used to align the second-order statistic correlation information between two distributions with a non-linear transformation. Suppose the feature covariance matrices of source and target domains are $C^S$ and $C^T$, and the number of source and target data are $n^S$ and $n^T$, respectively. The deepCoral loss $\ell_{coral}$ can be expressed by:

$$\ell_{coral} = \frac{1}{4d^2}\|C^S - C^T\|_F^2 \quad (5)$$

where $\|\cdot\|_F^2$ represents the squared matrix Frobenius norm, and $d$ denotes the dimension of the features. The covariance matrices of source and target data can be calculated by:

$$C^S = \frac{1}{n^S-1}\left(\boldsymbol{X}^{S\top}\boldsymbol{X}^S - \frac{1}{n^S}(\mathbf{1}^\top\boldsymbol{X}^S)^\top(\mathbf{1}^\top\boldsymbol{X}^S)\right) \quad (6)$$

$$C^T = \frac{1}{n^T-1}\left(\boldsymbol{X}^{T\top}\boldsymbol{X}^T - \frac{1}{n^T}(\mathbf{1}^\top\boldsymbol{X}^T)^\top(\mathbf{1}^\top\boldsymbol{X}^T)\right) \quad (7)$$

where $\mathbf{1}$ represents a column vector with all elements equal to 1. Suppose $\boldsymbol{X}_{ij}^S$ and $\boldsymbol{X}_{ij}^T$ indicate the $j$-th dimension of the $i$-th source and target data, respectively. The gradient in terms of the input features can be obtained by:

$$\frac{\partial \ell_{coral}}{\partial \boldsymbol{X}_{ij}^S} = \frac{1}{d^2(n^S-1)}\left(\left(\boldsymbol{X}^{S\top} - \frac{1}{n^S}\left(\left(\mathbf{1}^\top\boldsymbol{X}^S\right)^\top\mathbf{1}^\top\right)^\top\left(C^S - C^T\right)\right)\right)^{ij} \quad (8)$$

$$\frac{\partial \ell_{coral}}{\partial \boldsymbol{X}_{ij}^T} = \frac{1}{d^2(n^T-1)}\left(\left(\boldsymbol{X}^{T\top} - \frac{1}{n^T}((\mathbf{1}^\top\boldsymbol{X}^T)^\top\mathbf{1}^\top)^\top\left(C^S - C^T\right)\right)\right)^{ij} \quad (9)$$

The batch covariances and the network parameters are shared between two ResNet-50 networks.

### C. Joint Loss for Knowledge Transfer

Our aim is to transfer the knowledge of DMs from the

labeled source data to the unlabeled target data and diagnosis the DMs from the unlabeled data. As shown in Fig. 1, a representation can be learned by minimizing the distance between the source and target data distributions, and a classifier of DMDM on the source domain with labeled data can be trained, which can be directly applied to the target unlabeled data with minimal loss in accuracy. However, minimizing the classification loss alone could lead to overfitting to the source domain and causing poor performance in target performance; minimizing the deepCoral loss alone might lead to degenerated features. To learn the features that work well on the target domain, we propose to use the joint loss with both classification loss $\ell_{class}$ and deepCoral loss $\ell_{coral}$ as the following:

$$\ell = \ell_{class} + \lambda \ell_{coral} \quad (10)$$

where $\lambda$ is a weighting factor for adapting the classification accuracy on the source domain. Since $\ell_{class}$ and $\ell_{coral}$ play counterparts, once an equilibrium is reached, the final features are expected to work well on the target domain.

## IV. Experiment Setup

### A. Dataset Preparation

#### 1) Synthetic and Real Datasets

The publicly available synthetic LFP battery dataset [19] is the only dataset that provides both DMs and voltage vs. capacity curves with over 700,000 unique curves, collected with one commercial battery, A123 2.3Ah ANR26650M. The LFP and graphite electrodes are matched with an LR of 0.95, OFS of 12.5%, and a resistance adjustment of −0.07 to match the A123 ANR26650M experimental data. The mechanistic framework is used as a backward modeling approach where the input is the degradation and the outputs are the battery's voltage and capacity. Also, it is compiled with a resolution of 0.01 for the triplets and C/25 charges. Each path is simulated with at most 0.85% increases for each degradation mode up to 85%. The synthetic dataset contains the whole degradation process of capacity from 100% to 0%, and the battery is considered to be unstable when capacity is lower than 80%. To learn the full features with capacity ≥ 80%, transfer learning is conducted for the capacity greater than 75% with 412,477 unique curves. We divide the entire synthetic dataset **S** into three parts (**S1**, **S2**, **S3**) with the same number of curves. Since each curve is unique, neither part contains a curve from the other parts.

The real LFP battery dataset containing batteries, A123 1.1Ah APR18650M1A, cycled to 80% capacity with different temperatures and C-rates [34] can be downloaded from https://www.batteryarchive.org/index. html. Note that the actual charging C-rate is greater than 0.5, which is different from that of C/25 for the synthetic dataset. To evaluate the transfer learning performance for DMDM, we select the following four sets of battery data cycled under different conditions as **R1** (a battery with temperature of 25℃ and C-rate of 1C), **R2** (a battery with temperature of 15℃, and C-rate of 1C), **R3** (a battery with temperature of 25℃ and C-rate of 2C), and **R4** (a battery with temperature of 25℃ and C-rate of 3C), respectively.

In order to show the difference in feature distribution between the synthetic and real datasets, the depth of the negative peak in $\Delta Q(V)$ is selected as a feature (x-axis), of which the distributions are plotted as the following figures. From Figs. 3 (1)-(3), we can find the distributions of peak depth in $\Delta Q(V)$ are different because **S** is classified sequentially rather than randomly into three parts to ensure the existence of distribution differences. The distributions of **R** are different from those of **S** in terms of the distribution range since the battery used in **S** is LFP A123 2.3Ah ANR26650 M and in **R** is LFP A123 1.1Ah APR18650M1A. In addition, due to the different operating temperatures and C-rate, the distributions of **R1**, **R2**, **R3**, and **R4** are also different.

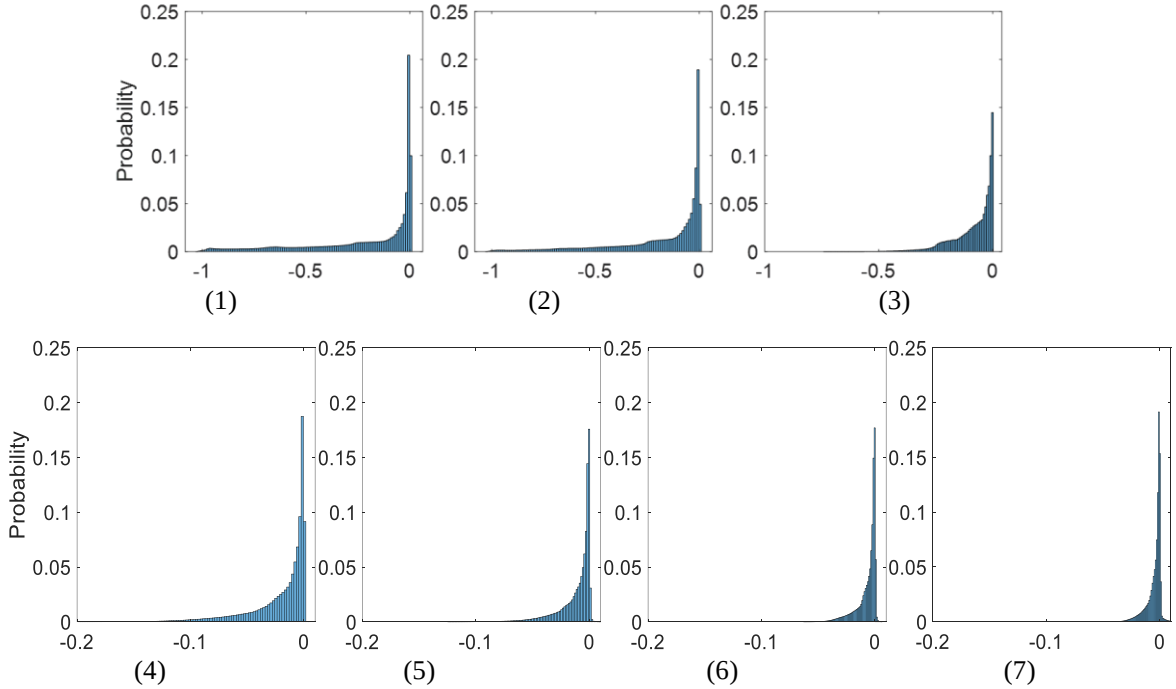


Fig. 3. Distribution of peak depth in $\Delta Q(V)$ for the synthetic and real datasets: (1)-(3) **S1-S3**; (4)-(7) **R1-R4**.

*2) Data Preprocessing*

Since the voltage and capacity curves of the real battery dataset are actual measurements that contain noise, a filter is introduced to remove the noise. This step is unnecessary for the synthetic dataset.

The effective features of the $\Delta Q(V)$ curves are generally concentrated between 2.2 V and 3.6 V. The measured voltages are commonly sampled at the same time interval, but the voltage intervals are inconsistent. The linear interpolation is employed to ensure consistent voltage intervals for both synthetic and real datasets.

The previous works commonly transformed the original incremental capacity images into one-dimensional data as the input. This commonly leads to the loss of some features and thus poor accuracy. As a result, some changes or shifts in the peak and valley positions are usually used to determine the DMs of the battery. In this work, the two-dimensional $\Delta Q(V)$ curve images are binarized and then used directly as the input of DMDM.

The output of DMDM is the classification of DMs, which contain the LLI, $\text{LAM}^{\text{PE}}$, and $\text{LAM}^{\text{NE}}$. The degradation path, which is simulated with at most 0.85% increases for each degradation mode up to 85%, can be divided into ten classes. We use subscript numbers to indicate the class of DMs as:

$$\begin{cases} LLI = \{LLI_0, LLI_1, \cdots, LLI_9\} \\ LAM^{PE} = \{LAM^{PE}{}_0, LAM^{PE}{}_1, \cdots, LAM^{PE}{}_9\} \\ LAM^{NE} = \{LAM^{NE}{}_0, LAM^{NE}{}_1, \cdots, LAM^{NE}{}_9\} \end{cases} \quad (11)$$

where $LLI_0$ denotes that the current LLI is between 0 and 8.5%, and $LAM^{PE}{}_9$ denotes that the current $\text{LAM}^{\text{PE}}$ is between 76.5% and 85%. Since we only consider the DMs corresponding to the capacity greater than 75%, after analyzing all synthetic datasets, the types of DMs that correspond to the capacity less than 75% are excluded. For a total of 120 combinations of DMs, the final classification is

$$\begin{cases} LLI = \{LLI_0, LLI_1, LLI_2\} \\ LAM^{PE} = \{LAM^{PE}{}_0, LAM^{PE}{}_1, \cdots, LAM^{PE}{}_3\} \\ LAM^{NE} = \{LAM^{NE}{}_0, LAM^{NE}{}_1, \cdots, LAM^{NE}{}_9\} \end{cases} \quad (12)$$

## B. Verification of DM Knowledge Transferability

*1) Transfer Learning within Synthetic Dataset*

Classification accuracy as a widely used metric that summarizes the performance of DMDM is given by:

$$acc = \frac{N^{correct}}{N^{total}} \quad (13)$$

where $N^{correct}$ denotes the number of correct classifications and $N^{total}$ represents the total number of samples in the test set.

*2) Transfer Learning from Synthetic to Real Dataset*

Our research aims to transfer knowledge from synthetic datasets to real datasets. Real battery datasets do not contain real DMs because these DMs are co-reacted by complex electrochemical reactions and are difficult to calculate quantitatively. Current DMs can be obtained by disassembling the batteries, but once the batteries are disassembled or damaged, the degradation process is suspended, and the subsequent paths cannot be obtained. Although there is no labeled real dataset that can be directly used to test the classification accuracy, we design the validation session with the classification accuracy as an intermediate variable and verify the classification accuracy by comparing the improvement of SOH brought by the DM classification as shown in Fig. 4.

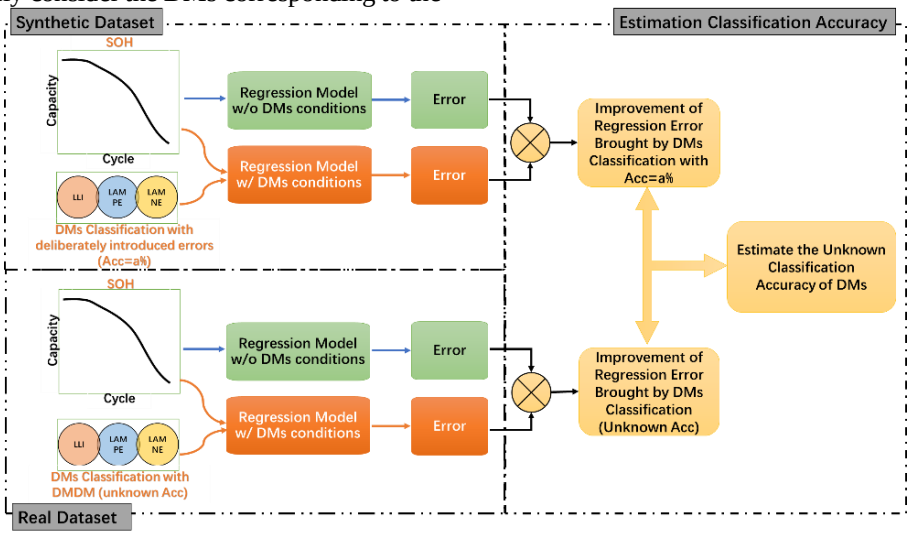


Fig. 4. The verification approach for DM classification accuracy from synthetic dataset to real dataset

First, a DM generation program is proposed with the labeled synthetic dataset, which can deliberately introduce inaccurate DMs so that the total DM accuracy varies from 0% to 100% with an interval of 5%. Then, we train several SOH regression models, which can estimate next SOH with historical SOHs as input, all of which have the same parameters and structures; the only difference is whether the inputs contain DMs with different accuracy or not. After that, the models are trained separately to obtain the regression errors with or without DMs at different accuracies. Taking the regression error without DMs as the benchmark, dividing the error with different DMs by the benchmark can obtain the improvements brought by DMs. Also, a mapping between DM classification accuracy and regression error can be obtained. Using the DMs obtained by knowledge transfer DMDM as the input and repeating the above steps, we can calculate the regression error. In combination with the mapping obtained above, the DM classification accuracy can be estimated.

## V. Case Studies and Discussion

### A. Different Settings Effects

Selecting appropriate settings of the DMDM is essential to transfer knowledge and classify DM accuracy. We evaluate the model performance on task **S1** → **S2**, which contains 137,492 paths, to select the reasonable neural networks, domain adaptation loss, weighting factor, and inputs of DMDM.

*1) Selection of Different Neural Networks*

The classification neural network is the most important part of the DMDM model that determines the accuracy of the classification. Here, we introduce several commonly used deep neural networks, including the convolutional neural networks (CNN), recurrent neural network (RNN), AlexNet, ResNets with different layers (ResNet-18, ResNet-34, ResNet-101, and ResNet-152), and UNet combined with RestNet-50 and CNN (Res-UNet and CNN-UNet), to compare the classification accuracy and time cost. Fig. 5 shows the average accuracy and training time of task **S1→ S2** with ResNet-50 and other neural networks. As shown, ResNets with more than 50 layers (ResNet-50, ResNet-101, and ResNet-152) and Res-UNet can provide a relatively high classification accuracy with more than 85%, followed by CNN-UNet, AlexNet, and ResNet-34 with more than 60% accuracy, while CNN and RNN show the poorest performance (approximately 20%). However, ResNet-101, ResNet-152, and Res-UNet require more training time than ResNet-50, without significantly improving the classification accuracy. Hence, we choose ResNet-50 as the classification model in this paper. In order to make ResNet classification more accurate, the hyperparameters are optimized by multiple simulations in the order of batch size, learning rate, momentum, and weight delay, with the range [128, 256, 512, 1024] (batch size), [0.01, 0.05, 0.1, 0.2, 0.4, 0.8] (learning rate), [0.01, 0.05, 0.1, 0.2, 0.4 ,0.8] (momentum), and [0.0001, 0.0005, 0.001, 0.002, 0.004] (weight delay). The optimal values of the batch size, learning rate, momentum, and weight delay are determined as 512, 0.1, 0.2, and 0.004, respectively.

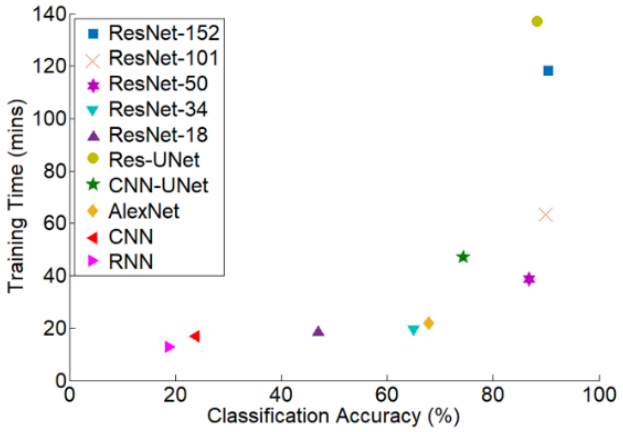


Fig. 5. Comparison of DM classification accuracies and training time with different deep networks

*2) Selection of Domain Adaptation Loss*

Another essential part is the loss of domain adaptation transfer learning, which is used to evaluate the distance between the source domain and the target domain. Three domain adaptation losses, the Batch Nuclear-norm Maximization (BNM) [35], Maximum Mean Discrepancy (MMD), and Local MMD (LMMD) [36], are introduced to compare with the deepCoral loss. Fig. 6 illustrates the training and test accuracies for training with different domain adaptation losses. It is shown that the deepCoral loss can achieve much better performance on the target domain **S2** with about 85%, while LMMD and BNM are just more than 40%. However, all the four losses maintain strong classification accuracy on the source domain with almost 93%. This demonstrates that the deepCoral loss is more suitable for DM knowledge transfer in DMDM models.

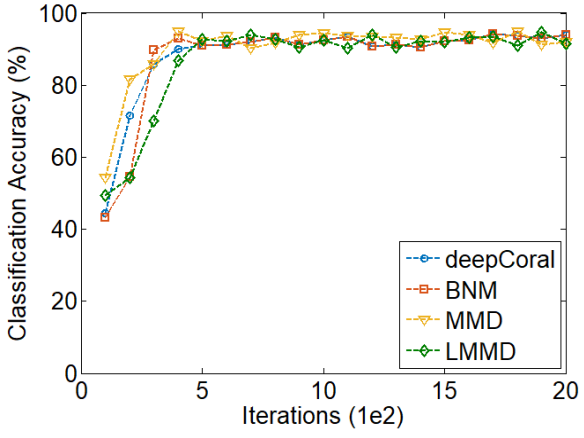


(a)

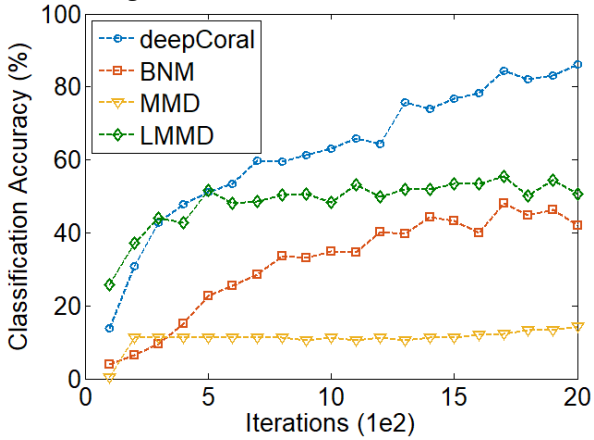


(b)

Fig. 6. Comparison of DM classification accuracies with different adaptation losses, (a) training (b) test

*3) Selection of Weighting Factor λ*

Another critical parameter is the weight loss $\lambda$, which is used to balance the classification loss and adaptation loss. Fig. 7 transfer loss in terms of weight factor $\lambda$. As shown, if $\lambda$ is set too small, the domain adaptation will not impact the learned representation and transfer no useful feature to the target domain. On the other hand, a too large $\lambda$ will result in the degeneration of extracted features. As shown in Fig. 7, $\lambda$=1.5 gives a suitable trade-off to jointly optimize the classification and domain adaptation losses to learn the hidden features that can work well on the target domain to enhance the feature transferability and improve the DM classification accuracy. Therefore, in this paper, we set $\lambda$ to 1.5 for all experiments.

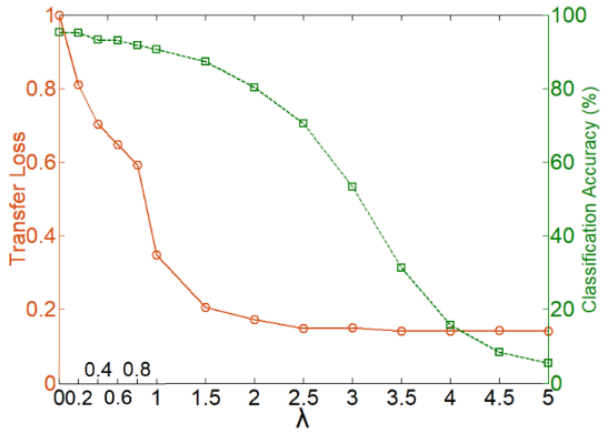


Fig. 7. Comparison of DM classification accuracies and transfer losses with different weighting factor $\lambda$

*4) Selection of Input of DMDM*

Many researchers applied IC curves with a low charging rate to analyze the DMs. This, however, disagrees with the situation in real-world applications where the charging rate is always high. Moreover, the charging images are transformed into sequences as the inputs to explore the relationship in previous work. We introduce images and sequences of $dQ/dV(V)$ and $\Delta Q(V)$ as the input of the DMDM model to do comparison experiments. Fig. 8 (a) shows the training classification accuracy of source domain **S1** with different inputs. It can be seen that even in the source domain, applying the images as the input of the DM classification model leads to relatively high accuracy, almost 1.4 times (94.23% for $\Delta Q(V)$ ) and 3.1 times (92.83% for $dQ/dV(V)$) higher than those using sequence as the input. Because data in the synthetic dataset are simulated with C/25, it is impossible to determine how effective $dQ/dV(V)$ and $\Delta Q(V)$ can be, but what can be sure is that using the image as the input can preserve more of the original features. We will explore which image input is more reasonable, $dQ/dV(V)$ or $\Delta Q(V)$, from low C-rate (C/25) to high C-rate (1C ~ 3C) with real datasets in subsection *V.C*. Fig. 8 (b) shows the training time for image-based and sequence-based inputs are 38.7 mins and 41.3 mins with the image-based input and 16.5 mins and 15.8 mins with the sequence-based input. One can find that the training time for image-based input is twice more than that with the sequence as input. However, for the **S1** dataset, the correct DM classification accuracy for the image as input is 94.23%, while the accuracy for the sequence as input is 67.32% and 30.14%. If one wants to improve the DM classification accuracy with the sequence-based $dQ/dV(V)$ input, the battery should be charged at a C-rate of 1/20, which means charging time consumption is 20 hours. Compared to 20 hours, the training time of 38.7 mins is acceptable. In addition, it should be pointed out that although it takes some time to train the image-based model, the entire training process is completely offline. Only a few seconds are required to output the classification results with a trained model.

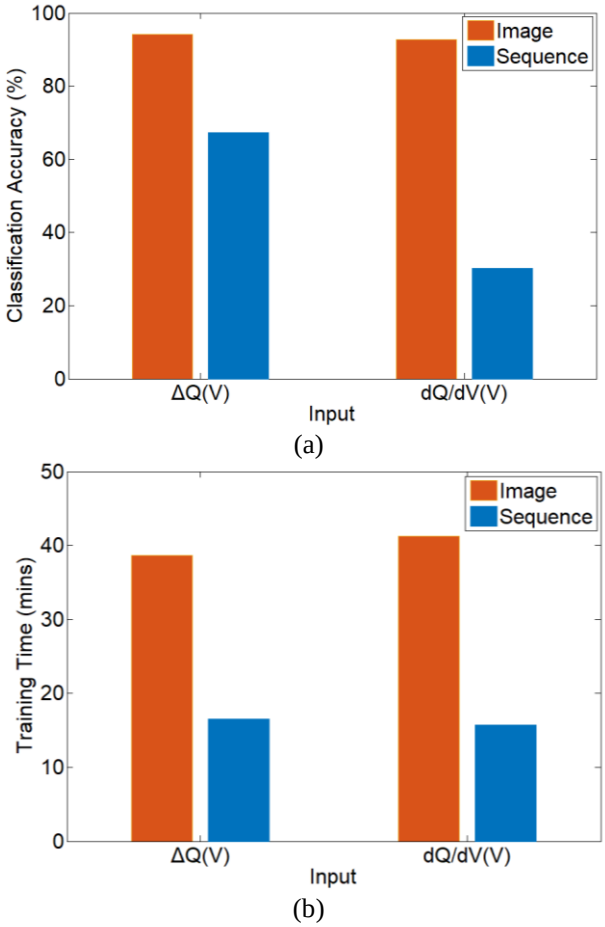


Fig. 8. Comparison of DM classification accuracies (a), and training time (b) in **S1** with images or sequences as the input

## *B. Domain Adaptation within Synthetic Dataset*

TABLE I COMPARISON OF DM CLASSIFICATION ACCURACY WITHIN THE SYNTHETIC DATASET

| Method | **S1 → S2** | **S1 → S3** | **S2 → S3** | **AVG** |
|---|---|---|---|---|
| Proposed | 84.73±3.48 | 83.60±2.16 | 80.38±4.82 | 82.90±3.49 |
| CNN | 22.42±7.38 | 18.71±4.93 | 19.63±6.37 | 20.25±6.23 |
| RNN | 17.73±6.97 | 14.83±2.05 | 16.77±4.96 | 16.44±4.66 |
| DAN | 68.11±9.19 | 62.93±6.08 | 58.63±11.32 | 63.22±7.64 |
| DAAN | 73.87±10.92 | 72.16±8.44 | 77.90±9.66 | 74.64±9.67 |
| DSAN | 58.89±4.01 | 67.43±5.93 | 62.14±4.05 | 62.82±4.99 |

In this subsection, to verify the transferability of DM knowledge within the synthetic dataset, the synthetic dataset is divided into three parts, and one of the three parts is selected sequentially to be the source domain and the other two to be the target domains. For the target domain, we randomly select 10,000 samples for testing. The proposed DMDM is compared to several recent domain adaptation methods: basic deep adaptation networks (DAN) [37], dynamic adversarial adaptation network (DAAN) [38], deep subdomain adaptation network (DSAN) [36], and two no adaptation DL methods: CNN and RNN. The hyperparameters and networks of DAN, DAAN and DSAN are the same as ResNet-50 in section *V.A.1)*.

Table I lists the average and standard deviation of the classification accuracy for **S1 → S2**, **S1 → S3**, and **S2 → S3**. One can find that the proposed method can achieve the highest DM classification accuracy after knowledge transfer with an average of 82.9. Compared with CNN and RNN without domain adaptation, the proposed method is able to increase the accuracy from almost 20% to more than 80%. Hence, the improvement of our method is significant. On the other hand, compared with the other three domain adaptation methods, the proposed DMDM also achieves better DM diagnosis ability.

### *C. Domain Adaptation from Synthetic Dataset to Real Dataset*

Although the proposed model has good knowledge transferability for the synthetic dataset, our aim is to transfer DM knowledge from the synthetic dataset to the real dataset, which can further improve the state analysis of the battery. However, the DMs of the real battery dataset are unseen. Therefore, we design a validation session in subsection *IV.B*. We follow the approach by deliberately introducing inaccurate DMs and collecting the regression error improvements brought by DMs with a long short term memory (LSTM) network. Fig. 9 shows a relationship between DM classification accuracy and improvement of SOH regression error. The orange scattered points represent that the DMs, with a classification accuracy of 60% or higher, are a positive gain to the regression error of SOH, and the blue points with a classification accuracy of 60% or lower show a negative gain for the regression model. The yellow dotted curve shows a smoothed fitting of the blue and yellow points with a high-order polynomial fitting function and can be used to verify the DM classification accuracy in a real dataset. For example, an improvement of 0.2 in regression error can yield a DM classification accuracy of 86% after domain adaptation.

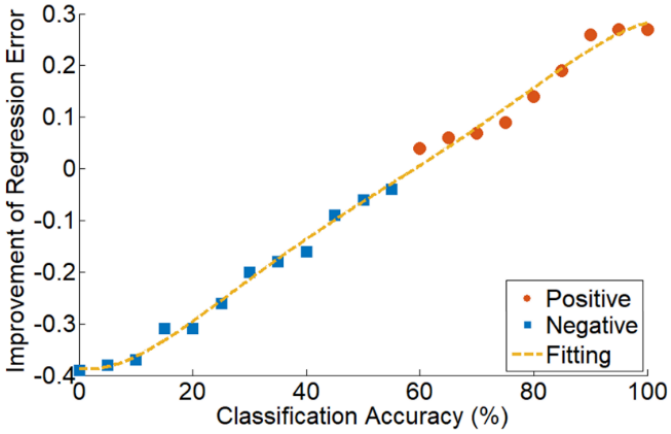


Fig. 9. The relationship between DM classification accuracy and improvement of SOH regression error

Table II tabulates the improvement of SOH regression error and estimated accuracy of the DMs from synthetic dataset to real dataset, including **S → R1**, **S → R2**, **S → R3**, and **S → R4**, with the proposed method, DAN, DAAN, DSAN, CNN, and RNN. In addition, to find out which image input is more reasonable for DM knowledge transferring from low C-rate (C/25) to high C-rate (1C ~ 3C), we apply $dQ/dV(V)$ and $\Delta Q(V)$, respectively, as the input of the DMDM model to do comparison experiments. The top underlined values in Table II denote the improvement of SOH regression error, and the bottom bold values denote the estimated DM classification accuracy.

TABLE II COMPARISON OF DMS CLASSIFICATION ACCURACY FROM SYNTHETIC DATASET TO REAL DATASET

| Method | S → R1 | | S → R2 | | S → R3 | | S → R4 | | AVG | |
|---|---|---|---|---|---|---|---|---|---|---|
| Input | $dQ/dV(V)$ | $\Delta Q(V)$ | $dQ/dV(V)$ | $\Delta Q(V)$ | $dQ/dV(V)$ | $\Delta Q(V)$ | $dQ/dV(V)$ | $\Delta Q(V)$ | $dQ/dV(V)$ | $\Delta Q(V)$ |
| Proposed | **53.51** | **79.26** | **48.49** | **76.92** | **18.38** | **73.92** | **19.40** | **70.61** | **34.95** | **75.18** |
| | -0.039 | 0.149 | -0.073 | 0.132 | -0.307 | 0.108 | -0.300 | 0.085 | | |
| CNN | **10.07** | **5.76** | **1.02** | **8.36** | **0.32** | **2.07** | **5.76** | **13.38** | **4.46** | **7.39** |
| | -0.360 | -0.381 | -0.391 | -0.371 | -0.392 | -0.389 | -0.381 | -0.343 | | |
| RNN | **0** | **2.27** | **10.03** | **8.03** | **0** | **0** | **0** | **10.37** | **2.51** | **5.17** |
| | -0.410 | -0.388 | -0.3623 | -0.372 | -0.418 | -0.482 | -0.441 | -0.360 | | |
| DAN | **35.12** | **55.85** | **44.48** | **57.62** | **19.05** | **51.92** | **27.68** | **50.84** | **31.58** | **54.06** |
| | -0.174 | -0.023 | -0.102 | -0.009 | -0.302 | -0.049 | -0.233 | -0.058 | | |
| DAAN | **46.82** | **60.20** | **55.18** | **60.67** | **30.43** | **57.19** | **21.74** | **54.84** | **38.54** | **58.23** |
| | -0.085 | 0.008 | -0.028 | 0.011 | -0.212 | -0.013 | -0.281 | -0.030 | | |
| DSAN | **22.41** | **48.83** | **37.79** | **50.34** | **12.36** | **48.49** | **3.68** | **47.16** | **19.06** | **48.71** |
| | -0.274 | -0.071 | -0.152 | -0.061 | -0.350 | -0.073 | -0.386 | -0.083 | | |

It can be found that the proposed method based on ResNet-50 and deepCoral shows the best performance with an average estimated classification accuracy of 75.18%, followed by DAAN with 58.23%, DAN with 54.06%, DSAN with 48.71%, and CNN with 7.39%, respectively. The RNN-based DM classification provides the worst negative gain for SOH regression error, and the average classification accuracy is 5.17%. As shown, applying $dQ/dV(V)$ and $\Delta Q(V)$ as the inputs to the model will have a significant impact on the classification accuracy. For **R1**, with a C-rate of 1C, the estimated accuracies are 53.51% ($dQ/dV(V)$) and 79.26% ($\Delta Q(V)$). For **R4** with a C-rate of 3C, the estimated accuracies are 19.40% ($dQ/dV(V)$) and 70.61% ($\Delta Q(V)$). This means that at a high C-rate, using $dQ/dV(V)$ as the input may lose more features, and when C-rate is 3C, the classification accuracy is only one-third of that with a C-rate of 1C. This demonstrates that $\Delta Q(V)$ is more suitable for DM transfer from low C-rate (C/25) to high C-rate (1C ~ 3C). Comparing the classification accuracies of **S → R1** and **S → R2**, one can find that with $\Delta Q(V)$ as the input, the accuracy is slightly smaller by 2.34%

with temperature = 15℃ (76.92%) than that with temperature = 25℃ (79.26%). This suggests that low temperature (15℃) can also affect DM transferability and lead to a slight decrease in DM classification accuracy.

## VI. Conclusion and Further work

In this paper, the quantitative DM diagnosis problem for LFP battery was first proposed. A deep domain adaptation method is proposed for DM knowledge transferability. Various comparative experiments are conducted to determine the most suitable DL model, domain adaptation loss, structure, and parameters. Using the images of $\Delta Q(V)$ as the input leads to a significant improvement in DM classification performance. The proposed deep domain adaptation for the DMDM method is successfully applied to transfer DMs from synthetic datasets to real datasets across different LFP battery types. In future work, we will try to transfer the knowledge of DMs from LFP to other types of Li-ion batteries, such as nickel manganese cobalt (NMC) and nickel cobalt aluminum (NCA). The performance of proposed model will be conducted under dynamic operation conditions for the real batteries. We will also study DMs from an EM point of view to directly verify the effectiveness of the proposed domain adaptation transfer learning.

## VII. References


[1] B. Gou, Y. Xu, and X. Feng, "State-of-health estimation and remaining-useful-life prediction for lithium-ion battery using a hybrid data-driven method," *IEEE Transactions on Vehicular Technology,* vol. 69, no. 10, pp. 10854-10867, 2020.

[2] L. Zheng, J. Zhu, D. D.-C. Lu, G. Wang, and T. He, "Incremental capacity analysis and differential voltage analysis based state of charge and capacity estimation for lithium-ion batteries," *Energy,* vol. 150, pp. 759-769, 2018.

[3] H. Miao, G. Chen, C. Li, Z. Y. Dong, and K. P. Wong, "Operating expense optimization for EVs in multiple depots and charge stations environment using evolutionary heuristic method," *IEEE Transactions on Smart Grid,* vol. 9, no. 6, pp. 6599-6611, 2017.

[4] Y. Zhang, Y. Xu, H. Yang, Z. Y. Dong, and R. Zhang, "Optimal whole-life-cycle planning of battery energy storage for multi-functional services in power systems," *IEEE Transactions on Sustainable Energy,* vol. 11, no. 4, pp. 2077-2086, 2019.

[5] W. Liu, Y. Xu, and X. Feng, "A hierarchical and flexible data-driven method for online state-of-health estimation of li-ion battery," *IEEE Transactions on Vehicular Technology,* vol. 69, no. 12, pp. 14739-14748, 2020.

[6] W. Chen, J. Qiu, and Q. Chai, "Customized Critical Peak Rebate Pricing Mechanism for Virtual Power Plants," *IEEE Transactions on Sustainable Energy,* vol. 12, no. 4, pp. 2169-2183, 2021.

[7] C. R. Birkl, M. R. Roberts, E. McTurk, P. G. Bruce, and D. A. Howey, "Degradation diagnostics for lithium ion cells," *Journal of Power Sources,* vol. 341, pp. 373-386, 2017.

[8] A. Ahmadian, M. Sedghi, B. Mohammadi-ivatloo, A. Elkamel, M. A. Golkar, and M. Fowler, "Cost-benefit analysis of V2G implementation in distribution networks considering PEVs battery degradation," *IEEE Transactions on Sustainable Energy,* vol. 9, no. 2, pp. 961-970, 2017.

[9] E. Wikner, E. Björklund, J. Fridner, D. Brandell, and T. Thiringer, "How the utilised SOC window in commercial Li-ion pouch cells influence battery ageing," *Journal of Power Sources Advances,* vol. 8, pp. 100054, 2021.

[10] W. Yan, B. Zhang, W. Dou, D. Liu, and Y. Peng, "Low-cost adaptive lebesgue sampling particle filtering approach for real-time li-ion battery diagnosis and prognosis," *IEEE Transactions on Automation Science and Engineering,* vol. 14, no. 4, pp. 1601-1611, 2017.

[11] L. Zheng, J. Zhu, G. Wang, D. D.-C. Lu, and T. He, "Lithium-ion battery instantaneous available power prediction using surface lithium concentration of solid particles in a simplified electrochemical model," *IEEE Transactions on Power Electronics,* vol. 33, no. 11, pp. 9551-9560, 2018.

[12] M. Dubarry, C. Truchot, and B. Y. Liaw, "Synthesize battery degradation modes via a diagnostic and prognostic model," *Journal of power sources,* vol. 219, pp. 204-216, 2012.

[13] J. Li, K. Adewuyi, N. Lotfi, R. G. Landers, and J. Park, "A single particle model with chemical/mechanical degradation physics for lithium ion battery State of Health (SOH) estimation," *Applied energy,* vol. 212, pp. 1178-1190, 2018.

[14] R. Xiong, L. Li, Z. Li, Q. Yu, and H. Mu, "An electrochemical model based degradation state identification method of Lithium-ion battery for all-climate electric vehicles application," *Applied energy,* vol. 219, pp. 264-275, 2018.

[15] Y. Zhang, Q. Tang, Y. Zhang, J. Wang, U. Stimming, and A. A. Lee, "Identifying degradation patterns of lithium ion batteries from impedance spectroscopy using machine learning," *Nature communications,* vol. 11, no. 1, pp. 1-6, 2020.

[16] E. Kwak, S. Jeong, J.-h. Kim, and K.-Y. Oh, "Prediction of compression force evolution over degradation for a lithium-ion battery," *Journal of Power Sources,* vol. 483, pp. 229079, 2021.

[17] S. Kim, Z. Yi, B.-R. Chen, T. R. Tanim, and E. J. Dufek, "Rapid failure mode classification and quantification in batteries: A deep learning modeling framework," *Energy Storage Materials*, 2021.

[18] K. S. Mayilvahanan, K. J. Takeuchi, E. S. Takeuchi, A. C. Marschilok, and A. C. West, "Supervised Learning of Synthetic Big Data for Li‐Ion Battery Degradation Diagnosis," *Batteries & Supercaps,* vol. 5, no. 1, pp. e202100166, 2022.

[19] M. Dubarry, and D. Beck, "Big data training data for artificial intelligence-based Li-ion diagnosis and prognosis," *Journal of Power Sources,* vol. 479, pp. 228806, 2020.

[20] M. Dubarry, and D. Beck, "Analysis of synthetic voltage vs. capacity datasets for big data Li-ion diagnosis and prognosis," *Energies,* vol. 14, no. 9, pp. 2371, 2021.

[21] I. Oyewole, A. Chehade, and Y. Kim, "A controllable deep transfer learning network with multiple domain adaptation for battery state-of-charge estimation," *Applied Energy,* vol. 312, pp. 118726, 2022.

[22] T. Han, Z. Wang, and H. Meng, "End-to-end capacity estimation of Lithium-ion batteries with an enhanced long short-term memory network considering domain adaptation," *Journal of Power Sources,* vol. 520, pp. 230823, 2022.

[23] H. Chun, J. Kim, M. Kim, J. Lee, T. Lee, and S. Han, "Capacity estimation of lithium-ion batteries for various aging states through knowledge transfer," *IEEE Transactions on Transportation Electrification*, 2021.

[24] E. Tzeng, J. Hoffman, N. Zhang, K. Saenko, and T. Darrell, "Deep domain confusion: Maximizing for domain invariance," *arXiv preprint arXiv:1412.3474*, 2014.

[25] M. Dubarry, "Graphite//LFP synthetic V vs. Q dataset (>700,000 unique curves)," *Mendeley Data*, 2021.

[26] K. A. Severson, P. M. Attia, N. Jin, N. Perkins, B. Jiang, Z. Yang, M. H. Chen, M. Aykol, P. K. Herring, and D. Fraggedakis, "Data-driven prediction of battery cycle life before capacity degradation," *Nature Energy,* vol. 4, no. 5, pp. 383-391, 2019.

[27] D. Anseán, M. Dubarry, A. Devie, B. Liaw, V. García, J. Viera, and M. González, "Fast charging technique for high power LiFePO4 batteries: A mechanistic analysis of aging," *Journal of Power Sources,* vol. 321, pp. 201-209, 2016.

[28] D. Anseán, M. Dubarry, A. Devie, B. Liaw, V. García, J. Viera, and M. González, "Operando lithium plating quantification and early detection of a commercial LiFePO4 cell cycled under dynamic driving schedule," *Journal of Power Sources,* vol. 356, pp. 36-46, 2017.

[29] S. J. Pan, and Q. Yang, "A survey on transfer learning," *IEEE Transactions on knowledge and data engineering,* vol. 22, no. 10, pp. 1345-1359, 2009.

[30] J. Lin, J. Ma, J. Zhu, and H. Liang, "Deep Domain Adaptation for Non-Intrusive Load Monitoring Based on A Knowledge Transfer Learning Network," *IEEE Transactions on Smart Grid*, 2021.

[31] P. Westermann, M. Welzel, and R. Evins, "Using a deep temporal convolutional network as a building energy surrogate model that spans multiple climate zones," *Applied Energy,* vol. 278, pp. 115563, 2020.

[32] A. Nutkiewicz, Z. Yang, and R. K. Jain, "Data-driven Urban Energy

Simulation (DUE-S): A framework for integrating engineering simulation and machine learning methods in a multi-scale urban energy modeling workflow," *Applied energy,* vol. 225, pp. 1176-1189, 2018.

[33] B. Sun, and K. Saenko, "Deep coral: Correlation alignment for deep domain adaptation." *European conference on computer vision. Springer, Cham*, pp. 443-450,2016.

[34] Y. Preger, H. M. Barkholtz, A. Fresquez, D. L. Campbell, B. W. Juba, J. Romàn-Kustas, S. R. Ferreira, and B. Chalamala, "Degradation of commercial lithium-ion cells as a function of chemistry and cycling conditions," *Journal of The Electrochemical Society,* vol. 167, no. 12, pp. 120532, 2020.

[35] S. Cui, S. Wang, J. Zhuo, L. Li, Q. Huang, and Q. Tian, "Towards discriminability and diversity: Batch nuclear-norm maximization under label insufficient situations." pp. 3941-3950.

[36] Y. Zhu, F. Zhuang, J. Wang, G. Ke, J. Chen, J. Bian, H. Xiong, and Q. He, "Deep subdomain adaptation network for image classification," *IEEE transactions on neural networks and learning systems,* vol. 32, no. 4, pp. 1713-1722, 2020.

[37] M. Long, Y. Cao, J. Wang, and M. Jordan, "Learning transferable features with deep adaptation networks." *International conference on machine learning. PMLR*, pp. 97-105, 2015.

[38] C. Yu, J. Wang, Y. Chen, and M. Huang, "Transfer learning with dynamic adversarial adaptation network." *2019 IEEE International Conference on Data Mining (ICDM). IEEE,* pp. 778-786, 2019.

**Xin Lu** (Student Member, IEEE) received the B.E. degree in electricity engineering from Nanjing Institute of Technology, Jiangsu, China in 2013 and the M.E. degree in electrical engineering from Jiangnan University, Jiangsu, China in 2016. He is currently working toward the Ph.D. degree in electrical engineering with the University of Sydney, NSW, Australia. His areas of interest include electricity markets, pricing model, and power system operation and planning.

**Jing Qiu** (Senior Member, IEEE) is currently a Senior Lecturer in Electrical Engineering at the University of Sydney, Australia. He obtained his B.Eng. degree in control engineering from Shandong University, China, M.Sc. degree in environmental policy and management, majoring in carbon financing in the power sector, from The University of Manchester, U.K., and Ph.D. in electrical engineering from The University of Newcastle, Australia, in 2008, 2010 and 2014 respectively. His areas of interest include power system operation and planning, energy economics, electricity markets, and risk management. He is the Editorial Board Member of IET Energy Conversion and Economics.

**Gang Lei** (Member, IEEE) received the B.S. degree in Mathematics from Huanggang Normal University, China, in 2003, the M.S. degree in Mathematics and Ph.D. degree in Electrical Engineering from Huazhong University of Science and Technology, China, in 2006 and 2009, respectively. He is currently a Senior Lecturer at the School of Electrical and Data Engineering, University of Technology Sydney (UTS), Australia. His current research interests include electrical machines and systems, multidisciplinary design optimization, industrial big data and cloud computing techniques. He is an Associate Editor for the IEEE Transactions on Industrial Electronics and an Editor of the IEEE Transactions on Energy Conversion.

**Jianguo Zhu** (Senior Member, IEEE) received the B.E. degree in electrical engineering from the Jiangsu Institute of Technology, Jiangsu, China, in 1982, the M.E. degree in electrical engineering from the Shanghai University of Technology, Shanghai, China, in 1987, and the Ph.D. degree in electrical engineering from the University of Technology Sydney (UTS), Sydney, NSW, Australia, in 1995, where he was appointed as a Lecturer in 1994, and was promoted to a Full Professor in 2004, and a Distinguished Professor of Electrical Engineering in 2017. In 2018, he joined the University of Sydney, Australia, as a Full Professor and the Head of School for School of Electrical and Information Engineering. His research interests include computational electromagnetics, measurement and modeling of magnetic properties of materials, electrical machines and drives, power electronics, renewable energy systems, smart micro grids, and digital energy systems.